CHALMERS
UNIVERSITY OF TECHNOLOGY

Measurement of nuclear interaction cross sections towards neutron-skin thickness determination

Phys. Lett. B 855 (2024) 138780

Contents lists available at ScienceDirect

Physics Letters B

journal homepage: www.elsevier.com/locate/physletb

Letter

Measurement of nuclear interaction cross sections towards neutron-skin thickness determination

L. Ponnath [a,*,1], T. Aumann [b,c,d], C.A. Bertulani [e,b,d], R. Gernhäuser [a], M. Heil [c], T. Almusidi [f], H. Alvarez-Pol [g], L. Atar [b], L. Atkins [h], Y. Ayyad [g], J. Benlliure [g], K. Boretzky [c], M.J.G. Borge [i], L.T. Bott [j], G. Bruni [k], B. Brückner [j], P. Cabanelas [g], C. Caesar [c], E. Casarejos [l], J. Cederkall [m], A. Corsi [n], D. Cortina-Gil [g], J.A. Dueñas [o], M. Duer [b], Z. Elekes [p], S. Escribano Rodriguez [h], L. Fabbietti [a], A. Falduto [b], M. Feijoo [g], M. Feijoo Fontan [g], L.M. Fonseca [b], A. Frotscher [b], D. Galaviz [q,r], E. Galiana [q], G. García-Jiménez [g], I. Gašparić [s], E.I. Geraci [t,u], A. Gillibert [n], B. Gnoffo [t,u], D. González Caamaño [g], A. Graña González [g], K. Göbel [j,c], A.-L. Hartig [b], A. Heinz [k], T. Hensel [v], M. Holl [b], A. Horvat [b,s], A. Jedele [b,d], D. Jelavić Malenica [s], T. Jenegger [a], H.T. Johansson [k], B. Jonson [k], N. Kalantar-Nayestanaki [w], A. Kelic-Heil [c], O.A. Kiselev [c], P. Klenze [a], D. Kresan [c], T. Kröll [b], E. Kudaibergenova [b], D. Kurtulgil [j], D. Körper [c], M. Labiche [x], C. Langer [j,y], I. Lihtar [s], Yu.A. Litvinov [c], B. Löher [b,c], J. Mayer [z], S. Murillo Morales [h], E. Nacher [aa], T. Nilsson [k], A. Obertelli [b], V. Panin [c], J. Park [ab], S. Paschalis [h], A. Perea [i], M. Petri [h], S. Pirrone [u], T. Pohl [b], R. Reifarth [j], H.-B. Rhee [b], J.L. Rodriguez-Sanchez [g,2], L. Rose [h], D.M. Rossi [b,c], P. Russotto [ac], D. Savran [c], H. Scheit [b], H. Simon [c], S. Storck-Dutine [b], A.M. Stott [h], C. Sürder [b], R. Taniuchi [h], O. Tengblad [i], P. Teubig [q,r], L. Trache [ad], M. Trimarchi [u,ae], H.T. Törnqvist [b,c], L. Varga [a], V. Wagner [b], F. Wamers [c] for R^{3}B Collaboration

[a] Technische Universität München, School of Natural Science, James-Franck-Str 1, Garching, 85748, Germany
[b] Technische Universität Darmstadt, Fachbereich Physik, Institut für Kernphysik, 64289, Darmstadt, Germany
[c] GSI Helmholtzzentrum für Schwerionenforschung, Planckstraße 1, 64291, Darmstadt, Germany
[d] Helmholtz Forschungsakademie Hessen für FAIR (HFHF), GSI Helmholtzzentrum für Schwerionenforschung, Campus Darmstadt, 64289, Darmstadt, Germany
[e] Texas A&M University-Commerce, 75428, Commerce, TX, United States of America
[f] King Saud University, Riyadh, 11451, Saudi Arabia
[g] IGFAE, Universidade de Santiago de Compostela, Santiago de Compostela, E-15782, Spain
[h] School of Physics, Engineering and Technology, University of York, York, YO10 5DD, United Kingdom
[i] Instituto de Estructura de la Materia, CSIC, Madrid, E-28006, Spain
[j] Goethe-Universität Frankfurt, Max-von-Laue Str. 1, Frankfurt am Main, 60438, Germany
[k] Institutionen för Fysik, Chalmers Tekniska Högskola, Göteborg, 412 96, Sweden
[l] CINTECX, Universidade de Vigo, DSN, Dpt. Mech. Engineering, Vigo, E-36310, Spain
[m] Lund University, Department of Physics, P.O. box 118, Lund, 221 00, Sweden
[n] CEA Saclay, IRFU/DPhN, Centre de Saclay, Gif-sur-Yvette, 91191, France
[o] Depto. Ingeniería Eléctrica y Centro de Estudios Avanzados en Física, Matemáticas y Computación. Universidad de Huelva, Huelva, 21071, Spain
[p] ATOMKI Debrecen, Bem tér 18/c, Debrecen, 4026, Hungary
[q] Laboratório de Instrumentacão e Física Experimental de Partículas, LIP, Av. Prof. Gama Pinto 2, Lisbon, 1649-003, Portugal
[r] University of Lisbon - Faculdade de Ciencias, Campo Grande, Lisbon, 1649-016, Portugal
[s] RBI Zagreb, Bijenicka cesta 54, Zagreb, HR10000, Croatia
[t] Universitá di Catania, Dipartimento di Fisica e Astronomia "Ettore Majorana", Catania, Italy
[u] INFN Sezione di Catania, Via Santa Sofia 64, Catania, 95123, Italy
[v] Helmholtz-Zentrum Dresden-Rossendorf, Institute of Radiation Physics, Bautzner Landstraße 400, Dresden, 01328, Germany
[w] ESRIG, University of Groningen, Groningen, Netherlands
[x] Science and Technology Facilities Council - Daresbury Laboratory, Warrington, WA4 4AD, United Kingdom

* Corresponding author.
E-mail address: lponnath@ikp.tu-darmstadt.de (L. Ponnath).
[1] Present address: Technische Universität Darmstadt, Fachbereich Physik, Institut für Kernphysik, 64289 Darmstadt, Germany.
[2] Present address: CITENI, Campus Industrial de Ferrol, Universidade da Coruña, E-15403 Ferrol, Spain.

https://doi.org/10.1016/j.physletb.2024.138780
Received 7 January 2024; Received in revised form 17 May 2024; Accepted 3 June 2024
Available online 5 June 2024

[y] FH Aachen University of Applied Sciences, Aachen, 52066, Germany
[z] Universität zu Köln, Institut für Kernphysik, Zülpicher Straße 77, Köln, 50937, Germany
[aa] Instituto de Física Corpuscular (CSIC – Univ. of Valencia), Paterna (Valencia), E-46980, Spain
[ab] Center for Exotic Nuclear Studies, Institute for Basic Science, Daejeon, 34126, Republic of Korea
[ac] INFN Laboratori Nazionali del Sud, Via Santa Sofia 62, Catania, 95123, Italy
[ad] IFIN-HH, Bucharest, Romania
[ae] Università degli studi di Messina, Italy

ARTICLE INFO

Editor: B. Blank

ABSTRACT

The accuracy of reaction theories used to extract properties of exotic nuclei from scattering experiments is often unknown or not quantified, but of utmost importance when, e.g., constraining the equation of state of asymmetric nuclear matter from observables as the neutron-skin thickness. In order to test the Glauber multiple-scattering model, the total interaction cross section of ^{12}C on carbon targets was measured at initial beam energies of 400, 550, 650, 800, and 1000 MeV/nucleon. The measurements were performed during the first experiment of the newly constructed R^{3}B (Reaction with Relativistic Radioactive Beams) experiment after the start of FAIR Phase-0 at the GSI/FAIR facility with beam energies of 400, 550, 650, 800, and 1000 MeV/nucleon. The combination of the large-acceptance dipole magnet GLAD and a newly designed and highly efficient Time-of-Flight detector enabled a precise transmission measurement with several target thicknesses for each initial beam energy with an experimental uncertainty of $\pm 0.4\%$. A comparison with the Glauber model revealed a discrepancy of around 3.1% at higher beam energies, which will serve as a crucial baseline for the model-dependent uncertainty in future fragmentation experiments.

1. Introduction

A precise measurement of the neutron-skin thickness of exotic nuclei could provide experimental constraints on the symmetry energy at saturation density and thus on the equation of state (EOS) of asymmetric nuclear matter [1–3]. The EOS describes the physics of nuclear matter as a function of density and is thus essential to interpret astrophysical observations of neutron stars and to reproduce their properties such as mass-radius relation and gravitational-wave signatures in stellar modeling [4–6]. So far, the symmetry energy (E_{sym}) and especially its slope parameter $L = 3\rho_0 \delta E_{sym}(\rho)/\delta\rho|_{\rho_0}$ at saturation energy are experimentally only weakly constrained and vary over a wide range for different interactions in non-relativistic or relativistic mean-field models [3]. In this context, there is a strong experimental interest in measuring the neutron skin of exotic nuclei with high precision as proposed by various experiments employing different mechanisms [3,7–10]. The neutron skin of a nucleus is defined as the difference between the rms radii of its neutron and proton density distributions. The proton or charge distribution, especially of stable isotopes, is measured via electron scattering [11] and isotopic shift experiments [12] whereas the neutron or matter distribution, especially for neutron-rich and exotic nuclei, is very challenging to access since hadronic probes have to be employed to access the matter radii, which needs the use of nuclear-reaction models with quantified theoretical uncertainties. One of the experimentally simplest methods applicable to low-intensity radioactive beams is the measurement of the total interaction cross section. In the pioneering work of Tanihata et al. [13], reaction cross-section measurements have been established as a common technique to study the total nucleon density distribution of light neutron-rich nuclei. The highly spatially extended neutron density distribution was later interpreted as a neutron halo by Hansen and Jonson [14]. Since that time, reaction cross-section measurements have been widely carried out to investigate the density distribution of stable and exotic nuclei at radioactive-ion-beam facilities at intermediate [15–17] or at relativistic energies, e.g., at the GSI facility [18–20].

Since the total interaction cross section is dominated by the charge-changing cross section, where at least one proton was involved in a nucleon-nucleon (NN) scattering process, its sensitivity to the neutron-skin thickness is rather limited. In contrast, the total neutron-removal cross section probes the neutron density distribution [7,21]. A well-established method to describe integrated cross sections of nuclear reactions at high energies is the Glauber multiple scattering model [22].

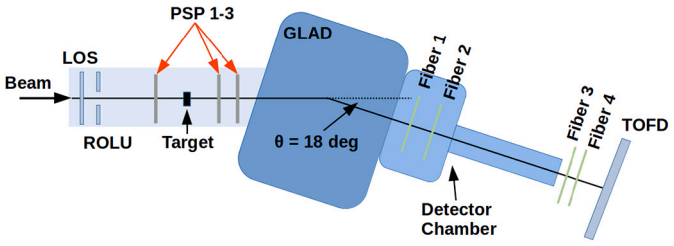

Fig. 1. Schematic view of R^{3}B experimental setup. Sizes are not to scale.

In such a realistic model, the only inputs are the experimental nucleon-nucleon cross sections and the proton and neutron density distributions. The later ones can be derived from density functional theories.

For a precise determination of the neutron-skin thickness, it is essential to quantify the uncertainty of the reaction model. The measurement of the total interaction cross sections of ^{12}C+ ^{12}C at relativistic energies represents the ideal case for a direct comparison with results based on a realistic reaction model, as presented in [23], since the charge density distribution is well known. In the energy regime between 400 and 1000 MeV/nucleon, there are currently just three experimental data points available [24–26]. Here we present a precise measurement of the total interaction cross section of ^{12}C+ ^{12}C at initial beam energies of 400, 550, 650, 800, and 1000 MeV/nucleon. The new data allows for a systematic comparison to state-of-the-art model calculations to test their level of accuracy and hence the predictive power.

2. Experiment

The S444 commissioning experiment of R^{3}B was the first experiment of the FAIR Phase-0 campaign in Cave-C at GSI. A stable ^{12}C beam was delivered from synchrotron SIS18 into Cave-C with an average intensity of 4×10^4 particles per second and chosen energies of 400, 550, 650, 800, and 1000 MeV/nucleon.

Fig. 1 shows a schematic view of the main systems of the R^{3}B setup used during this experiment. The start detector (LOS [27]) is followed by a veto detector (ROLU [27]), which excludes particles with a larger spatial offset to the beamline than its adjustable aperture. A set of three double-sided position-sensitive pin diode detectors (PSP) was installed in the setup in order to make a charge and position identification before and after the target. PSP 1 was installed 0.8 m upstream of the fixed target/reaction point. PSP 2 was mounted 0.8 m after the target

Table 1
Target thickness d, number of scattering centers per unit area N_t and corresponding uncertainties for all carbon targets.

^{12}C targets	d [cm]	N_t [cm^{-2}]	ΔN_t [%]
thin	0.5451(4)	$5.059\,005 \times 10^{22}$	0.0648
medium	1.0793(15)	$1.001\,685 \times 10^{23}$	0.2620
thick	2.1928(5)	$2.035\,110 \times 10^{23}$	0.0322

and PSP 3 with a displacement of 0.2 m further downstream. GLAD is a zero-degree superconducting dipole magnet with a large angular acceptance (±80 mrad for neutrons) and an adjustable integrated magnetic field of at most 5 Tm [28]. The GLAD current and thus the magnetic field strength was adjusted for each beam energy individually to deflect the ^{12}C beam onto the 18-degree line with respect to the incoming beam. In order to cover an extensive program of more than 40 different beam/target combinations, the magnet setting was not changed to compensate for different energy losses in different targets. For the particle tracking after the magnetic field of GLAD, four fiber detectors were used. All four have an active area of 50 × 50 cm^2 consisting of 1024 square-shaped fibers with a thickness of 500 µm. Two of them - Fibers 1 and 2 - were placed inside the detector chamber perpendicular to the 18-degree line with a relative distance of 1.5 m. Fiber 3 and Fiber 4 were mounted right after the exit window of the vacuum pipe, with Fiber 4 rotated by 90 degrees to measure the vertical position. At the very end of the setup, perpendicular to the 18-degree line, a time-of-flight wall (TOFD) [29] was installed. In the used configuration, TOFD consisted of 4 planes with 44 vertical scintillator paddles each (1000 × 27 × 5 mm^3). Planes were shifted with respect to the adjacent plane by half a paddle. To minimize multiple scattering, the particles were propagated in vacuum from the beam entry of the cave to the magnet, its detector chamber and the connected vacuum pipe with a diameter of 60 cm on the fragment arm. About 1.5 m after the beam exit window, only the last two fiber detectors and the TOFD scintillator wall were operated in air.

The interaction cross section was determined via the conventional transmission method [30] where σ_I is expressed by:

$$\sigma_I = -\frac{1}{N_t} \ln\left(\frac{N_2^i/N_1^i}{N_2^o/N_1^o}\right) = -\frac{1}{N_t} \ln\left(\frac{R_i}{R_o}\right), \quad (1)$$

where $R_{i/o}$ are the ratios of the number of non-interacted nuclei after the target $N_2^{i/o}$ and the number of incoming nuclei $N_1^{i/o}$, for a target-in (i) and a target-out (o) run. The target-out run takes into account reactions within the setup material. N_t is the number of scattering centers per unit area which is defined as $N_t = \rho \cdot d \cdot N_A/M$, where N_A is the Avogadro constant, d is the target thickness in beam direction and M is the molar mass of natural carbon (12.0107 u), where we assumed a 1.07$ contribution of ^{13}C. Due to the relatively small difference in the reaction cross section of ^{13}C+ ^{12}C and ^{12}C+ ^{12}C [26], this contributes a maximum deviation of 0.02% between our results and theoretical calculations, considering the significant error bars reported in [26]. The volume density (ρ) of the carbon target material, manufactured by "SGL Carbon SE" [31] and specified by the GSI target lab, is 1.851(2) g cm^{-3}. Table 1 lists the values for d, N_t and corresponding statistical uncertainties based on the measured inhomogeneities of the target thickness (ΔN_t).

The number of incoming nuclei (N_1) was measured with detectors upstream of the target, namely LOS, ROLU, and PSP 1. A strict event selection was done using these systems by measuring the charge, position on the target and the time difference between consecutive particles.

The strategy to measure the number of non-interacting nuclei (N_2) in the present analysis is to minimize the systematic uncertainties by reducing the number of utilized detectors. In first order, just one detector, the TOFD time-of-flight wall was used to identify all carbon isotopes within the acceptance at the end of the setup $N_{Q=6}^{TOFD}$. Fig. 2 shows the identified charge in plane 1 vs plane 2 for a run with the medium ^{12}C target. The condition for an identified carbon isotope with the TOFD detector ($N_{Q=6}^{TOFD}$) is fulfilled if either plane 1 or plane 2 has measured a particle with charge 6 ± 0.5. By this, the dependency on the local gap size between paddles and the effect of different incident angles is avoided. Additionally, with this condition, even the tails of the Gaussian distributed carbon spot are considered within the cut, while the influence of the detector resolution on the result is minimized.

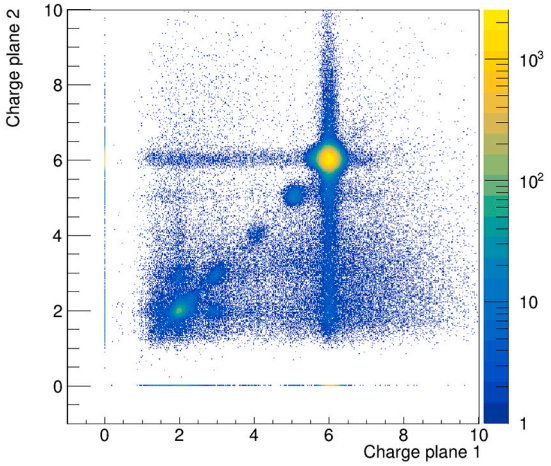

Fig. 2. Measured charge in TOFD plane 1 versus plane 2 for a 400 MeV/nucleon ^{12}C beam and the medium carbon target.

To validate the efficiency of the carbon identification, TOFD can be virtually divided into two identical separate detectors (detector 1 = plane 1 and 2, detector 2 = plane 3 and 4). The efficiency for the carbon identification $\epsilon_{Q=6}^{TOFD}$ was determined for each run individually to avoid position- or energy-dependent uncertainties.

By measuring only the nuclear charge in the first step, this number also includes other carbon isotopes than ^{12}C. In a second step, the ratio of ^{12}C isotopes compared to all identified carbon isotopes within the geometrical acceptance of TOFD ($R_{^{12}C}$) was determined for each run separately. For the separation of carbon isotopes, the residual velocity of projectiles after the target can be considered constant due to the approximately same energy loss within the setup material. Additionally, in the case of light nuclei like ^{11}C and ^{12}C, the mass-to-charge ratio difference is around 10%. Therefore, to identify the mass of a carbon particle entering the magnetic field of GLAD, it is sufficient to measure the horizontal position in front of and after GLAD. This was done using the PSP detectors after the target and the fiber detectors in the detector chamber after GLAD. The left panel of Fig. 3 shows both horizontal position measurements. The two diagonal distributions represent the ^{12}C and ^{11}C isotopes, respectively. The horizontal band indicates particles scattered in the setup material between PSP 3 and Fiber 1. By applying the condition that TOFD has registered a particle with charge 6 ± 0.5, this background is removed in the right panel of Fig. 3, where it is also visible that most of the ^{11}C distribution is bent to larger angles due to their lower mass. Thus, most ^{11}C are not reaching the geometrical acceptance window of the TOFD detector at the very end of the setup. The ratio of ^{12}C isotopes within the carbon data of TOFD is defined as

$$R_{^{12}C} = \frac{N_{^{12}C} \cdot \epsilon_{TOFD,PSP,Fib}}{N_{Q6} \cdot \epsilon_{TOFD,PSP,Fib}} = \frac{N_{^{12}C}}{N_{Q6}}, \quad (2)$$

where N_{Q6} is the total number of events in the right panel of Fig. 3. Two subsets of the same data are divided, where both depend on exactly the same efficiencies. Therefore, $R_{^{12}C}$ is independent of the rate- and time-dependent efficiency of the detectors.

An important correction factor for the geometrical acceptance A_C of the TOFD detector for ^{12}C isotopes needs to be determined. The effect

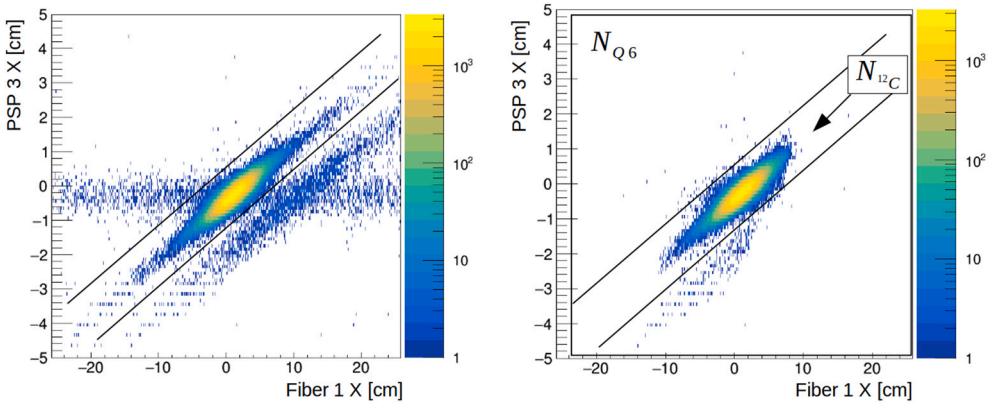

Fig. 3. Horizontal position of carbon ions at the PSP 3 in front of GLAD versus the horizontal position from Fiber 1 after the magnetic field of GLAD. The right panel shows the correlated positions under the additional conditions that TOFD registered a particle with charge 6 ± 0.5 in the same event.

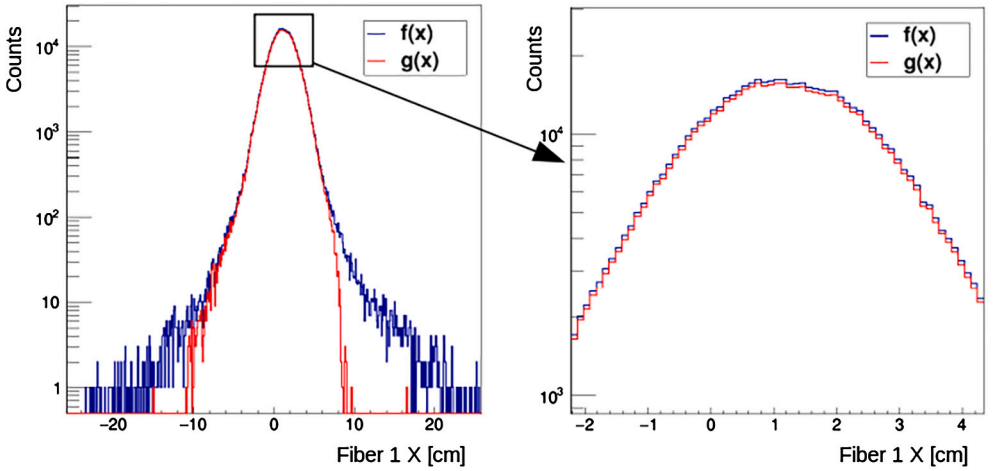

Fig. 4. Full (left) and peak region (right) of the ^{12}C distributions in the Fiber 1 horizontal plane. The blue graph - f(x) - is the distribution with just the PSP-Q = 6 condition, whereas the red graph - g(x) - is the same data set with the additional TOFD-Q = 6 condition.

of the limited geometrical acceptance of the experimental setup is illustrated in Fig. 3. After applying the TOFD-charge-condition on the data set, the edges of the ^{12}C distribution are cut off in the right panel.
Using the number of particles which are lost due to the limited geometrical acceptance $N_{^{12}C,mis.}$, it is possible to define the ratio of all identified carbon isotopes with TOFD (N^{TOFD}_{Q6}) and the full/reconstructed ^{12}C distribution as the following:

$$A_C = \frac{N^{TOFD}_{Q6,\epsilon(Fib,PSP)}}{N_{^{12}C,mis.,\epsilon(Fib,PSP)} + N^{TOFD}_{Q6,\epsilon(Fib,PSP)}}, \tag{3}$$

where the indices $\epsilon(\mathrm{Fib,PSP})$ indicate that all quantities depend on the same rate- and time-dependent efficiency of the fiber and PSP detectors.

The left panel in Fig. 4 compares the ^{12}C distribution (as illustrated in Fig. 3) with just the PSP-Q = 6 condition in blue and the additional TOFD Q = 6 condition in red. By zooming into the peak region (right panel), it can be seen that besides the hard cut-off of the distribution tails, the statistics also decrease in the central region after applying the TOFD condition. This effect is related to reactions within the remaining setup material between Fiber 1 and the TOFD detector. Reactions within the setup material are excluded by dividing a target-run by an empty-run (see Eq. (1)) and should not be corrected in this step. To use the blue "full-acceptance" distribution f(x) as a template for the limited-acceptance ^{12}C distribution g(x) in red, it has to be scaled down to compensate for the reactions in the remaining setup material.
The following relation defines the scaling factor:

$$S = \frac{\int_{x_{min}}^{x_{max}} g_{\epsilon(Fib,PSP)}(x)\,dx}{\int_{x_{min}}^{x_{max}} f_{\epsilon(Fib,PSP)}(x)\,dx} \tag{4}$$

x_{min} and x_{max} are a lower and upper limit for the central region (see Fig. 4), where the drop of statistics is not affected by the limited geometrical acceptance but just by reactions in the setup material. This factor has to be defined for each beam energy and target individually. Since g(x) is a subset of f(x), the time- and rate-dependent efficiencies of Fiber 1 and PSP 3 ($\epsilon(\mathrm{Fib,PSP})$) are the same and cancel out. Therefore, the scaling factor S is not efficiency dependent.
The derived scaling factor is used to compensate for the statistical difference between g(x) and f(x) caused by reactions within the setup material. The number of ^{12}C isotopes that are lost due to the geometrical acceptance can be calculated as:

$$N_{^{12}C,mis.} = \int_{Fib_{min}}^{Fib_{max}} f(x)\cdot S\,dx - \int_{Fib_{min}}^{Fib_{max}} g(x)\,dx\,, \tag{5}$$

where Fib_{max} and Fib_{min} indicate the area of the one-dimensional ^{12}C distribution in Fig. 4 which is affected by the limited geometrical acceptance. Eqs. (3) to (5) are used to define the factor A_C, which is the ratio of identified carbon isotopes with TOFD compared to the fully reconstructed ^{12}C distribution.

The final expression for the number of non-reacted ^{12}C particles reads:

Table 2
The measured total interaction cross sections (σ_I) for all different beam and target combinations together with the independent statistical ($\Delta\sigma_{stat.}$) and systematic contributions ($\Delta\sigma_{sys.}$).

Beam Energy [MeV/nucleon]	^{12}C targets	σ_I [mb]	$\Delta\sigma_{stat.}$ [mb]	$\Delta\sigma_{sys.}$ [mb]
400	thin	760.7(71)	5.38	4.62
	medium	764.6(44)	3.73	2.40
	thick	758.6(26)	1.84	1.87
550	thin	791.9(90)	8.10	4.07
	medium	795.8(53)	4.71	2.54
	thick	797.0(27)	2.46	1.23
650	thin	813.1(73)	6.20	3.78
	medium	811.5(57)	5.32	2.23
	thick	815.0(26)	2.28	1.35
800	medium	831.9(59)	5.23	2.74
	thick	834.6(33)	2.96	1.52
1000	thin	837.5(82)	7.40	3.49
	medium	836.1(56)	5.10	2.27
	thick	838.1(25)	2.25	1.14

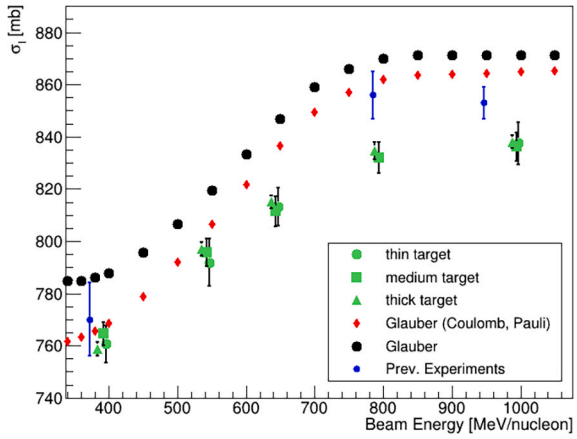

Fig. 5. Total interaction cross sections of ^{12}C+ ^{12}C versus beam energy. Experimental data for all target beam combinations (green symbols) are compared with calculations based on a reaction model - with (red symbols) and without in-medium corrections (black symbols) - and data from previous experiments (blue symbols) by Takechi et al. [25], Tanihata et al. [24], and Ozawa et al. [26].

$$N_2^{i/o} = \frac{N_{Q=6}^{TOFD}}{\epsilon_{Q=6}^{TOFD}} \cdot \left(1 - (1 - R_{^{12}C}) + \left(\frac{1}{A_C} - 1\right)\right). \quad (6)$$

3. Discussion

Table 2 and Fig. 5 show the measured cross sections for all target and beam energy combinations (green symbols). The independent statistical ($\Delta\sigma_{stat.}$) and systematic contribution ($\Delta\sigma_{sys.}$) are also listed in Table 2. All results are in agreement with the corresponding measurements with targets of different thicknesses within the given uncertainties and were used to challenge the nuclear reaction model.

We have used the Glauber theory method, described in Ref. [23] to obtain the reaction cross sections for ^{12}C+ ^{12}C collisions. The model includes (a) Pauli blocking, (b) Fermi motion, (c) higher-order eikonal corrections, (d) Coulomb repulsion, (e) relativistic corrections, and (f) nuclear excitation of giant resonances. In the case of ^{12}C+ ^{12}C, it has been shown that Pauli-blocking in nucleon-nucleon scattering is the main source of corrections to the Glauber model, see Ref. [23] for more details of the theory. The black circles in Fig. 5 represent calculations without in-medium corrections. Calculations, including Coulomb repulsion and Pauli blocking, are represented by the red diamonds. The blue circles denote results from previous experiments by Takechi et al. [25] (370 MeV/nucleon), Tanihata et al. [24] (790 MeV/nucleon), and Ozawa et al. [26] (950 MeV/nucleon).

The present measurements agree with the in-medium corrected Glauber model up to 550 MeV/nucleon. Our data indicate a softer rise of the cross section for higher energies and are 3.1% smaller than the model calculations including in-medium corrections at maximum energy.

4. Summary and conclusions

The presented total interaction cross sections of ^{12}C+ ^{12}C collisions with a total experimental uncertainty of down to $\pm 0.4\%$ represent the most precise currently available data in this energy range. The enhanced transparency of the ^{12}C nucleus at higher energies could not be explained in the Glauber reaction model so far and can be further studied with this precise data systematically. The increasing discrepancy between the presented experimental data and theory with the beam energy indicates an in-medium suppression of reaction processes. A further investigation of this effect is essential to reveal the origin and understand how it scales with the mass number or isospin asymmetry. As a conclusion of the presented analysis, a model-dependent uncertainty of at least 3.1% has to be considered for the determination of the neutron-skin thickness using a Glauber reaction model without any additional or free parameters. Assuming an experimental uncertainty of 1% for the measurement of total neutron-removal cross sections along the tin isotopic chain, the L parameter can be constrained to around ± 16MeV for ^{124}Sn and ± 10MeV for ^{132}Sn [7]. However, precise data on heavier systems would be very valuable to test the mass- and isospin dependence of the deviations before concluding on the model dependence for extracting a neutron-skin thickness and L-value range from the neutron-removal cross sections.

Declaration of competing interest

The authors declare that they have no known competing financial interests or personal relationships that could have appeared to influence the work reported in this paper.

Data availability

Data will be made available on request.

Acknowledgements

Results presented here are based on the experiment S444/S473, which was performed at the beamline infrastructure Cave-C at the GSI Helmholtzzentrum für Schwerionenforschung, Darmstadt (Germany) in the context of FAIR Phase-0. The project was supported by BMBF 05P21WOFN1, 05P19WOFN1, 05P21RDFN2, 05P19RDFN1, HFHF ("Helmholtz Forschungsakademie Hessen für FAIR") and funded by the Deutsche Forschungsgemeinschaft (DFG, German Research Foundation) under Germany's Excellence Strategy – EXC 2094 – 390783311. C.A.B. acknowledges support by the U.S. DOE grant DE- FG02-08ER41533. E.C acknowledges the support by the Spanish AEI PGC2018-099746-B-C22. J. Park acknowledges the support by the Institute for Basic Science (IBS-R031-D1). This work has been partly supported by the Spanish Funding Agency for Research (AEI) through Projects No. PID2019-104390GB-I00. I.G., A.H, D.J.M. and I.L. have been supported by Croatian Science Foundation (HRZZ) under project no. 1257. Supported by Portuguese FCT Project EXPL/FIS-NUC/0364/2021. J.L.R.S. thanks the support from Xunta de Galicia under the program of postdoctoral fellowships ED481B-2017-002 and ED481D-2021-018, and by the Grant No. RYC2021-031989-I. T.A., Y.A.L, and A.O. thank the State of Hesse within the Research Cluster ELEMENTS through project ID 500/10.006. Support by the Swedish Research Council under Contract

No. 2022-04248, 2014-06644-VR and 2021-04576-VR. This research was supported in part by the ExtreMe Matter Institute EMMI at the GSI Helmholtzzentrum fuer Schwerionenforschung, Darmstadt, Germany.

References

[1] B.A. Brown, Neutron radii in nuclei and the neutron equation of state, Phys. Rev. Lett. 85 (25) (2000) 5296.
[2] S. Typel, B.A. Brown, Neutron radii and the neutron equation of state in relativistic models, Physical Review C 64 (2) (2001) 027302.
[3] X. Roca-Maza, M. Centelles, X. Vinas, M. Warda, Neutron skin of Pb 208, nuclear symmetry energy, and the parity radius experiment, Phys. Rev. Lett. 106 (25) (2011) 252501.
[4] J.M. Lattimer, M. Prakash, The physics of neutron stars, Science 304 (5670) (2004) 536–542.
[5] J.M. Lattimer, The nuclear equation of state and neutron star masses, Annu. Rev. Nucl. Part. Sci. 62 (2012) 485–515.
[6] A. Sorensen, et al., Dense nuclear matter equation of state from heavy-ion collisions, arXiv preprint arXiv:2301.13253, 2023.
[7] T. Aumann, C. Bertulani, F. Schindler, S. Typel, Peeling off neutron skins from neutron-rich nuclei: constraints on the symmetry energy from neutron-removal cross sections, Phys. Rev. Lett. 119 (26) (2017) 262501.
[8] D. Rossi, et al., Measurement of the dipole polarizability of the unstable neutron-rich nucleus Ni 68, Phys. Rev. Lett. 111 (24) (2013) 242503.
[9] C. Bertulani, T. Aumann, et al., Maris polarization in neutron-rich nuclei, Phys. Lett. B 778 (2018) 30–34.
[10] J. Yang, J. Piekarewicz, Difference in proton radii of mirror nuclei as a possible surrogate for the neutron skin, Physical Review C 97 (1) (2018) 014314.
[11] H. De Vries, C. De Jager, C. De Vries, Nuclear charge-density-distribution parameters from elastic electron scattering, At. Data Nucl. Data Tables 36 (3) (1987) 495–536.
[12] B. Maaß, et al., Nuclear charge radii of ^{10,11}B, Phys. Rev. Lett. 122 (May 2019) 182501.
[13] I. Tanihata, H. Hamagaki, O. Hashimoto, Y. Shida, N. Yoshikawa, K. Sugimoto, O. Yamakawa, T. Kobayashi, N. Takahashi, Measurements of interaction cross sections and nuclear radii in the light p-shell region, Phys. Rev. Lett. 55 (24) (1985) 2676.
[14] P. Hansen, B. Jonson, The neutron halo of extremely neutron-rich nuclei, Europhys. Lett. 4 (4) (1987) 409.
[15] W. Mittig, J. Chouvel, Z.W. Long, et al., Measurement of total reaction cross sections of exotic neutron-rich nuclei, Phys. Rev. Lett. 59 (17) (1987) 1889.
[16] R. Warner, J. Kelley, P. Zecher, et al., Evidence for a proton halo in 8B: enhanced total reaction cross sections at 20 to 60 Mev/nucleon, Physical Review C 52 (3) (1995) R1166.
[17] M. Fukuda, T. Ichihara, N. Inabe, T. Kubo, H. Kumagai, T. Nakagawa, Y. Yano, I. Tanihata, et al., Neutron halo in 11Be studied via reaction cross sections, Phys. Lett. B 268 (3–4) (1991) 339–344.
[18] T. Suzuki, H. Geissel, et al., Neutron skin of Na isotopes studied via their interaction cross sections, Phys. Rev. Lett. 75 (18) (1995) 3241.
[19] T. Suzuki, H. Geissel, et al., Nuclear radii of Na and Mg isotopes, Nucl. Phys. A 630 (3–4) (1998) 661–677.
[20] L. Chulkov, G. Kraus, et al., Interaction cross sections and matter radii of A= 20 isobars, Nucl. Phys. A 603 (2) (1996) 219–237.
[21] C. Bertulani, J. Valencia, Neutron skins as laboratory constraints on properties of neutron stars and on what we can learn from heavy ion fragmentation reactions, Physical Review C 100 (1) (2019) 015802.
[22] C. Bertulani, P. Danielewicz, Introduction to Nuclear Reactions, CRC Press, 2021.
[23] E.A. Teixeira, T. Aumann, C. Bertulani, B. Carlson, Nuclear fragmentation reactions as a probe of neutron skins in nuclei, Eur. Phys. J. A 58 (10) (2022) 1–16.
[24] I. Tanihata, in: Proceedings of the First International Conference on Radioactive Nuclear Beams: 16-18 October 1989, Lawrence Berkeley Laboratory, World Scientific Publishing Company Incorporated, 1990, p. 477.
[25] M. Takechi, M. Fukuda, M. Mihara, K. Tanaka, T. Chinda, et al., Reaction cross sections at intermediate energies and Fermi-motion effect, Physical Review C 79 (Jun. 2009) 061601.
[26] A. Ozawa, O. Bochkarev, L. Chulkov, D. Cortina, H. Geissel, et al., Measurements of interaction cross sections for light neutron-rich nuclei at relativistic energies and determination of effective matter radii, Nucl. Phys. A 691 (3) (2001) 599–617.
[27] Technical report for the design construction and commissioning of the tracking detectors for R^{3}B, GSI Helmholtzzentrum fur Schwerionenforschung, November 2014.
[28] B. Gastineau, A. Donati, J.-E. Ducret, et al., Design status of the R^{3}B-GLAD magnet: large acceptance superconducting dipole with active shielding, graded coils, large forces and indirect cooling by thermosiphon, IEEE Trans. Appl. Supercond. 18 (2) (2008) 407–410.
[29] M. Heil, A. Kelić-Heil, L. Bott, et al., A new time-of-flight detector for the R^{3}B setup, Eur. Phys. J. A 58 (12) (2022) 1–19.
[30] I. Tanihata, H. Savajols, R. Kanungo, Recent experimental progress in nuclear halo structure studies, Prog. Part. Nucl. Phys. 68 (2013) 215–313.
[31] SGL Carbon SE, Wiesbaden, Germany, Grade R 6650 / Specialty Graphites, https://www.sglcarbon.com/.